Dynamical processes in hard-sphere fluids

B. Kamgar-Parsi,* E. G. D. Cohen, and I. M. de Schepper†
The Rockefeller University, 1230 York Avenue, New York, New York 10021-6399
(Received 13 January 1987)

For a classical fluid of hard spheres the nine hydrodynamic time-correlation functions between the microscopic density, longitudinal velocity, and temperature are calculated theoretically on the basis of the revised Enskog theory for all densities and wave numbers. It appears that a simplified description of these correlation functions is possible for small wave numbers in terms of extended hydrodynamic modes and for large wave numbers in terms of free streaming and a single binary collision.

I. INTRODUCTION

In the past years many studies have been made of the dynamical properties of classical fluids. In particular, one has studied the decay in time of density fluctuations, through the density-density correlation function, or its Fourier transform, the dynamic structure factor, which can be measured by light[1,2] or neutron scattering.[3–7] Special attention has been paid to hard-sphere fluids as a simple model for more realistic liquids.[8–17] The hope was that, just as for the static properties of fluids, hard-sphere-fluid studies might form a useful starting point and guideline for the understanding of real fluids, although important differences could be expected to occur. In this paper we report results of a rather complete theoretical investigation of a whole class of correlation functions, viz., those related to the hydrodynamic quantities: the density, longitudinal velocity, and temperature, for all hard-sphere fluid densities and all values of the wave number $k=2\pi/\lambda$, with λ the wavelength of the fluctuation. This way an overall picture of the dynamical behavior of fluctuations on a microscopic level in a fluid will be obtained and the transition from collective (i.e., hydrodynamic) behavior, for small k, to individual particle (i.e., ideal-gas) behavior for large k can be studied in detail.

This investigation was partly inspired by a determination of the nine hydrodynamic correlation functions of a hard-sphere fluid using computer simulations for three densities and an analysis in terms of a generalized hydrodynamic matrix given before by Alley, Alder, and Yip.[18,19] A detailed comparison with their results will be made below.

Our calculations are all based on a dynamical operator, the inhomogeneous Enskog operator $L_E(\mathbf{k})$, which describes approximately the time evolution of fluctuations with wave vector $\mathbf{k}$ in a hard-sphere fluid.[8–14] In fact, we will call a hard-sphere fluid described by this operator an Enskog fluid. We will see, however, that as far as presently available computer data on hard-sphere fluids are concerned, the Enskog fluid closely resembles a real hard-sphere fluid.[18–20]

Calculations of the density-density correlation function based on the inhomogeneous Enskog operator have been carried out before by others[12,18,19] as well as by ourselves.[13–15] The main difference between our work and that of others is that we have studied the time behavior of density fluctuations through the eigenmodes of the Enskog operator, i.e., through the eigenvalues and eigenfunctions which, in our approach, represent the basic dynamical processes in the fluid. We found, at high densities, that the dynamic behavior of density fluctuations could be understood on the basis of a particular class of eigenmodes of $L_E(\mathbf{k})$, viz., those that are obtained by extending the usual hydrodynamic modes—the eigenmodes of the linearized Navier-Stokes equations, in particular, the heat and sound modes—to larger values of k. The main difference between the present and our previous papers[13–17] is that apart from an extension to all nine hydrodynamic correlation functions, much better approximations have been used to obtain the eigenmodes of the operator $L_E(\mathbf{k})$. Although the basic conclusions of our previous papers do not change, a considerably more complicated picture in detail has emerged.

The main conclusion of this paper is that, globally, three density and four k regimes can be distinguished in the dynamical processes that dominate the hydrodynamic correlation functions. Introducing the volume V at close packing V_0, one distinguishes the following regimes:

(1) the dilute-gas regime $V_0/V<0.1$;
(2) the intermediate-density regime $0.1<V_0/V<0.35$;
(3) the dense-fluid regime $0.35<V_0/V<0.70$.

In each of these density regimes the dominant dynamical processes are associated with the following eigenmodes of $L_E(\mathbf{k})$:

(1) the kinetic analog of the three hydrodynamical (heat and sound) modes for $0\leqq kl_E<0.1$;
(2) their extensions, via $L_E(\mathbf{k})$, to larger values of k, i.e., for $0.1<kl_E<1$, as well as two more modes of $L_E(\mathbf{k})$ that are needed in the intermediate-density regime;
(3) a regime where all eigenmodes of $L_E(\mathbf{k})$ are needed and no simplified description exists: $1<kl_E<3$;
(4) a regime where the eigenmodes associated with individual-particle (free) streaming dominate and a single correction, due to one binary collision, suffices: $3<kl_E<\infty$.

Here l_E is the Enskog mean free path for a fluid of hard spheres: $l_E = l_0/\chi$, where $l_0 = 1/n\pi\sigma^2\sqrt{2}$ is the (Boltzmann) mean free path for a dilute gas of hard spheres of diameter σ and number density n, $\chi = g(\sigma)$, with $g(\sigma)$ the radial distribution function for two hard spheres at contact, and $V_0/V = n\sigma^3/\sqrt{2}$.

In Sec. II we review the basic formulas of the theory. In Sec. III the dilute-gas regime, in Sec. IV the dense-fluid regime, and in Sec. V the intermediate-density regime are discussed. In Sec. VI a discussion of the main results is presented. In particular, the density-density correlation function is considered and a comparison with previous work is made.

II. THE REVISED ENSKOG THEORY AND THE DETERMINATION OF EIGENMODES

A. N-particle time-correlation functions

For a fluid of hard spheres we consider the nine hydrodynamic time-correlation functions (with α or $\beta = 1,2,3$ and $t \geq 0$),

$$F_{\alpha\beta}(k,t) = \langle a_\alpha^*(\mathbf{k}) e^{tL} a_\beta(\mathbf{k}) \rangle_N , \tag{2.1}$$

where $\mathbf{k}$ is a wave vector with length $k = |\mathbf{k}| \neq 0$, the brackets $\langle \ldots \rangle_N$ indicate an equilibrium average over a canonical ensemble of N particles in a volume V at temperature T and density $n = N/V$, the star denotes complex conjugation, and L is the Liouville operator for hard spheres,[10,21,22]

$$L = \sum_{i=1}^{N} \mathbf{v}_i \cdot \frac{\partial}{\partial \mathbf{r}_i} + \sum_{\substack{i,j=1 \\ i<j}}^{N} T_{ij} , \tag{2.2}$$

where $\mathbf{v}_i$ and $\mathbf{r}_i$ denote the velocity and position of particle i at $t=0$, respectively. The first term in Eq. (2.2) describes the free streaming, while T_{ij} describes a binary collision between the particles i and j, i.e.,

$$T_{ij} = -\sigma \int d\hat{\sigma} \, |\mathbf{v}_{ij} \cdot \boldsymbol{\sigma}| \, \theta(\mathbf{v}_{ij} \cdot \boldsymbol{\sigma}) \delta(\mathbf{r}_{ij} + \boldsymbol{\sigma}) \times [1 - b_{\hat{\sigma}}(ij)] , \tag{2.3}$$

with $\mathbf{v}_{ij} = \mathbf{v}_i - \mathbf{v}_j$, $\mathbf{r}_{ij} = \mathbf{r}_i - \mathbf{r}_j$; $\hat{\sigma}$ a unit vector defining the geometry of the binary collision, $\boldsymbol{\sigma} = \sigma\hat{\sigma}$; $\theta(x)$ the Heaviside (step) function; and $b_{\hat{\sigma}}(ij)\mathbf{v}_i = \mathbf{v}_i' = \mathbf{v}_i - (\mathbf{v}_{ij} \cdot \hat{\sigma})\hat{\sigma}$ and $b_{\hat{\sigma}}(ij)\mathbf{v}_j = \mathbf{v}_j' = \mathbf{v}_j + (\mathbf{v}_{ij} \cdot \hat{\sigma})\hat{\sigma}$, with $\mathbf{v}_i'$ and $\mathbf{v}_j'$ the velocities after a collision of the particles i and j with initial velocities $\mathbf{v}_i$ and $\mathbf{v}_j$, respectively. For $k \neq 0$, the $a_\alpha(\mathbf{k})$ are the fluctuations of the conserved quantities, viz.,

$$a_1(\mathbf{k}) = \frac{1}{\sqrt{NS(k)}} \sum_{j=1}^{N} \phi_1(\mathbf{v}_j) e^{-i\mathbf{k}\cdot\mathbf{r}_j} \tag{2.4}$$

is the microscopic density fluctuation with $S(k)$ the static structure factor and $\phi_1(\mathbf{v}) = 1$;

$$a_2(\mathbf{k}) = \frac{1}{\sqrt{N}} \sum_{j=1}^{N} \phi_2(\mathbf{v}_j) e^{-i\mathbf{k}\cdot\mathbf{r}_j} \tag{2.5}$$

is the microscopic longitudinal velocity fluctuation with $\phi_2(\mathbf{v}) = (m/k_B T)^{1/2} \mathbf{k}\cdot\mathbf{v}/k$, m the mass of the particles, and k_B Boltzmann's constant; and

$$a_3(\mathbf{k}) = \frac{1}{\sqrt{N}} \sum_{j=1}^{N} \phi_3(\mathbf{v}_j) e^{-i\mathbf{k}\cdot\mathbf{r}_j} \tag{2.6}$$

is the microscopic temperature fluctuation with $\phi_3(\mathbf{v}) = (3 - mv^2/k_B T)/\sqrt{6}$.

We note that both the N-particle functions $a_\alpha(\mathbf{k})$, as well as the one-particle functions $\phi_\alpha(\mathbf{v})$ are orthonormal:

$$\langle a_\alpha^*(\mathbf{k}) a_\beta(\mathbf{k}) \rangle_N = \langle \phi_\alpha(\mathbf{v}_1) \phi_\beta(\mathbf{v}_1) \rangle_1 = \delta_{\alpha\beta} \quad (\alpha,\beta = 1,2,3) , \tag{2.7}$$

where the one-particle velocity average $\langle \ldots \rangle_1$ is defined, here and in the following, by

$$\langle h(\mathbf{v}_1) \rangle_1 = \int d\mathbf{v}_1 \, \phi(v_1) h(\mathbf{v}_1) , \tag{2.8}$$

for any function $h(\mathbf{v}_1)$ and $\phi(v_1)$ is the normalized Maxwell velocity distribution function

$$\phi(v) = \left(\frac{m}{2\pi k_B T} \right)^{3/2} e^{-mv^2/2k_B T} . \tag{2.9}$$

We also note that the set of correlation functions is symmetric in α and β, i.e., $F_{\alpha\beta}(k,t) = F_{\beta\alpha}(k,t)$ and depend on k only.

B. One-particle expressions

The class of N-particle time-correlation functions $F_{\alpha\beta}(k,t)$ defined in Eq. (2.1) can be approximately computed on the one-particle level using the revised Enskog theory.[8-11] The results $F_{\alpha\beta}^E(k,t)$ of that theory for $F_{\alpha\beta}(k,t)$ can be obtained from Eq. (2.1) by making three replacements:[23] (1) The N-particle average $\langle \ldots \rangle_N$ is replaced by the one-particle average $\langle \ldots \rangle_1$. (2) The N-particle Liouville operator L is replaced by a single-particle Enskog operator, for which various representations exist. While we have used before an asymmetric Enskog operator,[14,15] here a symmetric operator $L_E(\mathbf{k})$ (Ref. 23) will be used. (3) The N-particle functions $a_\alpha(\mathbf{k})$ are replaced by the one-particle functions $\phi_\alpha(\mathbf{v}_1)$. Then,

$$F_{\alpha\beta}^E(k,t) = \langle \phi_\alpha(\mathbf{v}_1) e^{tL_E(\mathbf{k})} \phi_\beta(\mathbf{v}_1) \rangle_1 , \tag{2.10}$$

where the (symmetric) inhomogeneous Enskog operator $L_E(\mathbf{k})$ acts on functions of the velocity $\mathbf{v}_1$ of a single particle and is given by

$$L_E(\mathbf{k}) = -i\mathbf{k}\cdot\mathbf{v}_1 + n\chi\bar{\Lambda}_\mathbf{k} + n\bar{A}_\mathbf{k} . \tag{2.11}$$

Here $-i\mathbf{k}\cdot\mathbf{v}_1$ represents the free streaming of the particle and the operator $\bar{\Lambda}_\mathbf{k}$ acts on an arbitrary function $h(\mathbf{v}_1)$ as

$$\bar{\Lambda}_\mathbf{k} h(\mathbf{v}_1) = \Lambda_\mathbf{k} h(\mathbf{v}_1) - \langle \Lambda_\mathbf{k} h(\mathbf{v}_1) \rangle_1 , \tag{2.12}$$

with the binary collision operator $\Lambda_\mathbf{k}$ given by

$$\Lambda_\mathbf{k} h(v_1) = \int d\mathbf{r}_2 \int d\mathbf{v}_2 \phi(v_2) T_{12} [h(\mathbf{v}_1) + e^{i\mathbf{k}\cdot\mathbf{r}_{21}} h(\mathbf{v}_2)] = -\sigma \int d\hat{\sigma} \int d\mathbf{v}_2 \phi(v_2) \, |\mathbf{v}_{12}\cdot\boldsymbol{\sigma}| \, \theta(\mathbf{v}_{12}\cdot\boldsymbol{\sigma}) \{ h(\mathbf{v}_1) - h(\mathbf{v}_1') + e^{-i\mathbf{k}\cdot\boldsymbol{\sigma}} [h(\mathbf{v}_2) - h(\mathbf{v}_2')] \} \tag{2.13}$$

and the mean-field operator $\bar{A}_{\mathbf{k}}$ given by

$$n\bar{A}_{\mathbf{k}}h(\mathbf{v}_1)=\left[1-\frac{1}{\sqrt{S(k)}}\right]\int d\mathbf{v}_2\,\phi(v_2)i\mathbf{k}\cdot(\mathbf{v}_1+\mathbf{v}_2)h(\mathbf{v}_2)\ . \tag{2.14}$$

We note that the $\mathbf{k}$ dependence of $\bar{\Lambda}_{\mathbf{k}}$ and $\bar{A}_{\mathbf{k}}$ is through $k\sigma$.[14] We note that on the one-particle level also the $F^E_{\alpha\beta}(k,t)$ are symmetric in α and β and depend on k only.[23]

C. The BGK method

(a) The time dependence of the $F^E_{\alpha\beta}(k,t)$, governed by the one-particle evolution operator $\exp[tL_E(\mathbf{k})]$ [cf. Eq. (2.10)], will be evaluated here using the Bhatnagar-Gross-Krook (BGK) method. In the BGK method,[12,14] the operator $L_E(\mathbf{k})$ is first converted into an ∞ matrix, using a complete set of functions, after which the Laplace transform of $\exp[tL_E(\mathbf{k})]$, i.e., the resolvent operator $[z-L_E(\mathbf{k})]^{-1}$, is inverted explicitly. Since the $F^E_{\alpha\beta}(k,t)$ only involve $v_1=|\mathbf{v}_1|$ and $\mathbf{k}\cdot\mathbf{v}_1$, a complete set of functions in v_1 and $\mathbf{k}\cdot\mathbf{v}_1$ only is needed. This is obtained by extending the set $\{\phi_\alpha(\mathbf{v}_1)\}$ with $\alpha=1,2,3$ to an infinite orthonormal set in v_1 and $\mathbf{k}\cdot\mathbf{v}_1$, $\{\phi_j(\mathbf{v}_1)\}$, defined below. Then the operator $L_E(\mathbf{k})$ is represented by the infinite matrix $\mathscr{L}^E(k)$ with elements

$$\mathscr{L}^E_{jl}(k)=\langle\phi_j(\mathbf{v}_1)L_E(\mathbf{k})\phi_l(\mathbf{v}_1)\rangle_1\ (j,l=1,2,\ldots,\infty)\ .$$

Choosing the z axis parallel to $\mathbf{k}$ and introducing a reduced velocity $\mathbf{c}=(m/2k_BT)^{1/2}\mathbf{v}$, we use the complete orthonormal set of functions,[24]

$$\phi_j(\mathbf{v})=\phi_{r,l}(\mathbf{v})=N_{r,l}c^lY_l^{(0)}(c_z/c)S^{(r)}_{l+1/2}(c^2)\ \ (j=r,l)\ . \tag{2.15}$$

Here $c=|\mathbf{c}|$; j stands for a pair of integers $r=0,1,2,\ldots$; $l=0,1,2,\ldots$; $Y_l^{(0)}(x)$ is the spherical harmonic $Y_l^{(m)}(x)$ with $m=0$; $S^{(r)}_{l+1/2}(c^2)$ is the Sonine polynomial of degree r with index $l+1/2$; and

$$N_{r,l}=\pi^{3/4}[2\Gamma(r+1)/\Gamma(r+l+3/2)]^{1/2}$$

is the normalization constant with $\Gamma(x)$ the gamma function. Thus

$$\langle\phi_{r_1,l_1}(\mathbf{v}_1)\phi_{r_2,l_2}(\mathbf{v}_1)\rangle_1=\delta_{r_1,r_2}\delta_{l_1,l_2}\ . \tag{2.16}$$

The first five ϕ_j are

$$\begin{aligned}
&\phi_1(\mathbf{v})=\phi_{0,0}(\mathbf{v})=1\ ,\\
&\phi_2(\mathbf{v})=\phi_{0,1}(\mathbf{v})=\sqrt{2}c_z\ ,\\
&\phi_3(\mathbf{v})=\phi_{1,0}(\mathbf{v})=\sqrt{2/3}(\tfrac{3}{2}-c^2)\ ,\\
&\phi_4(\mathbf{v})=\phi_{0,2}(\mathbf{v})=\sqrt{1/3}(3c_z^2-c^2)\ ,\\
&\phi_5(\mathbf{v})=\phi_{1,1}(\mathbf{v})=\sqrt{4/5}(\tfrac{5}{2}-c^2)c_z\ .
\end{aligned} \tag{2.17}$$

Here ϕ_1 represents the density, ϕ_2 the longitudinal velocity, ϕ_3 the temperature, while ϕ_4 and ϕ_5 are the kinetic parts of the z-z component of the stress tensor and the z component of the heat current, respectively.[23] The remaining polynomia can be ordered in different ways. We chose to order them according to the eigenvalues $\lambda_{r,l}$ of the Boltzmann collision operator $\Lambda_B=\lim_{k\to0}\Lambda_{\mathbf{k}}$ for hard spheres [cf. Eq. (3.2)] as computed by Alterman *et al.*[25]

(b) In the BGK approximation to $L_E(\mathbf{k})$ the free-streaming term $-i\mathbf{k}\cdot\mathbf{v}_1$ and the mean-field term $\bar{A}_{\mathbf{k}}$ are taken into account exactly. The collision operator $\bar{\Lambda}_{\mathbf{k}}$ is approximated by an infinite matrix with elements

$$\Omega_{jl}(k)=\langle\phi_j(\mathbf{v}_1)\bar{\Lambda}_{\mathbf{k}}\phi_l(\mathbf{v}_1)\rangle_1\ , \tag{2.18}$$

where in the BGK approximation of order M, the first $M\times M$ block of the matrix $\Omega_{jl}(k)$ $(j,l=1,2,\ldots,M)$ is taken into account exactly, while the remaining matrix elements $\Omega_{jl}(k)$ are set equal to zero, except for the diagonal elements $j=l=M+1,M+2,M+3,\ldots$, which are all set equal to $\Omega_{M+1,M+1}(k)=(n\chi)^{-1}d(k)$.

Then, in the Mth BGK approximation for $\bar{\Lambda}_{\mathbf{k}}$, the Enskog operator $L_E(\mathbf{k})$ is given by

$$L_E(\mathbf{k})=f(\mathbf{k})+F(\mathbf{k})\ , \tag{2.19}$$

where

$$f(\mathbf{k})=-i\mathbf{k}\cdot\mathbf{v}_1+d(k) \tag{2.20}$$

is a function of $\mathbf{v}_1$, while $F(\mathbf{k})$ is an operator acting on a function $h(\mathbf{v}_1)$ as

$$F(\mathbf{k})h(\mathbf{v}_1)=\sum_{j=1}^{M}\sum_{l=1}^{M}\phi_j(\mathbf{v}_1)\mathscr{F}_{jl}(k)\langle\phi_l(\mathbf{v}_1)h(\mathbf{v}_1)\rangle_1\ . \tag{2.21}$$

The $\mathscr{F}_{jl}(k)$ are elements of a symmetric $M\times M$ matrix $\mathscr{F}(k)$ given by

$$\mathscr{F}_{jl}(k)=-d(k)\delta_{jl}+n\chi\Omega_{jl}(k)+ik\left[\frac{k_BT}{m}\right]^{1/2}\left[1-\frac{1}{\sqrt{S(k)}}\right](\delta_{j1}\delta_{l2}+\delta_{j2}\delta_{l1})\ . \tag{2.22}$$

Here the term $-d(k)\delta_{jl}$ was obtained by first adding $d(k)$ to the diagonal matrix elements $\Omega_{jj}(k)$ for $j\leqq M$, where they were absent, and then extracting all the $d(k)$ diagonal elements of $L_E(\mathbf{k})$ and combining them with $-i\mathbf{k}\cdot\mathbf{v}_1$. The last term in Eq. (2.22) takes the mean-field term $\bar{A}_{\mathbf{k}}$ in $L_E(\mathbf{k})$ into account exactly. As a result, $L_E(\mathbf{k})$ is a sum of a multiplication operator $f(\mathbf{k})$ (which, equivalently, is an $\infty\times\infty$ matrix operator) and a *finite* $M\times M$ matrix operator $F(\mathbf{k})$. Such sums of multiplication and finite $M\times M$ matrix operators can be inverted explicitly for any M.

To compute now with the BGK method the nine correlation functions $F^E_{\alpha\beta}(k,t)$, we consider first the Laplace transforms:

$$G_{\alpha\beta}(k,z)=\int_0^\infty dt\, e^{-zt}F^E_{\alpha\beta}(k,t)$$
$$=\left\langle\phi_\alpha(\mathbf{v}_1)\frac{1}{z-L_E(\mathbf{k})}\phi_\beta(\mathbf{v}_1)\right\rangle_1$$
$$=\left[\frac{1}{z\mathbb{1}-\mathscr{L}^E(k)}\right]_{\alpha\beta}, \tag{2.23}$$

which are calculated by inverting the resolvent operator $1/[z-L_E(\mathbf{k})]$, with the BGK method, leading to the result

$$G_{\alpha\beta}(k,z)=\left[\frac{1}{\mathbb{1}-\mathscr{A}(k,z)\mathscr{T}(\mathbf{k})}\mathscr{A}(k,z)\right]_{\alpha\beta}. \tag{2.24}$$

Here $\mathscr{A}(k,z)$ is the $M\times M$ matrix with elements $\mathscr{A}_{jl}(k,z)$ given by $(j,l=1,\ldots,M)$:

$$\mathscr{A}_{jl}(k,z)=\left\langle\phi_j(\mathbf{v}_1)\frac{1}{z-f(\mathbf{k})}\phi_l(\mathbf{v}_1)\right\rangle_1$$
$$=\left\langle\phi_j(\mathbf{v}_1)\frac{1}{z+i\mathbf{k}\cdot\mathbf{v}_1-d(k)}\phi_l(\mathbf{v}_1)\right\rangle_1, \tag{2.25}$$

which can all be expressed in terms of the plasma dispersion function.[14,26]

The results that are quoted below are not for the correlation functions $F^E_{\alpha\beta}(k,t)$, but rather for their Fourier transforms:

$$S_{\alpha\beta}(k,\omega)=\frac{1}{2\pi}\int_{-\infty}^{\infty}dt\, e^{-i\omega t}F^E_{\alpha\beta}(k,t). \tag{2.26}$$

We note that only three of these are independent. We chose to calculate $(\alpha\beta)=(11)$, (13), and (33). Since these $F^E_{\alpha\beta}(k,t)$ are even functions of t, one can express these $S_{\alpha\beta}(k,\omega)$ in terms of the $G_{\alpha\beta}(k,z)$ by

$$S_{\alpha\beta}(k,\omega)=\frac{1}{\pi}\mathrm{Re}G_{\alpha\beta}(k,z)\,|_{z=i\omega}$$
$$=\frac{1}{\pi}\mathrm{Re}\left\langle\phi_\alpha(\mathbf{v}_1)\frac{1}{i\omega-L_E(\mathbf{k})}\phi_\beta(\mathbf{v}_1)\right\rangle_1. \tag{2.27}$$

We remark that the three $S_{\alpha\beta}(k,\omega)$ are even in ω, that the area $\int_{-\infty}^{\infty}d\omega S_{\alpha\beta}(k,\omega)$ is equal to 1 for $(\alpha\beta)=(11)$ and (33) and 0 for $(\alpha\beta)=(13)$ and that $S_{11}(k,\omega)=S(k,\omega)/S(k)$ with $S(k,\omega)$ the dynamic structure factor of the fluid.

(c) Thus the correlation functions $S_{\alpha\beta}(k,\omega)$ can be obtained directly from the $M\times M$ matrices $\mathscr{A}(k,z)$ and $\mathscr{T}(k)$ by matrix multiplication and inversion [cf. Eqs. (2.24) and (2.27)]. This has been done before for $S_{11}(k,\omega)$ by a number of authors.[12,14,19] To gain insight into the microscopic dynamical processes that dominate the correlation functions, we also evaluated the $S_{\alpha\beta}(k,\omega)$ by using the eigenmodes of $L_E(\mathbf{k})$. This is in the spirit of Landau-Placzek's theory of light scattering of fluids,[2] where $S(k,\omega)$ is computed in terms of the eigenmodes of the hydrodynamic Navier-Stokes equations. In this sense, our procedure is an extension of the Landau-Placzek theory of light scattering to neutron scattering and enables us to make a connection between the macroscopic properties of the fluid as expressed in the $F^E_{\alpha\beta}(k,t)$ and the microscopic properties of the fluid via its eigenmodes obtained from a one-particle (kinetic) representation of the $F^E_{\alpha\beta}(k,t)$.

D. Discrete BGK eigenmodes

The discrete eigenmodes of $L_E(\mathbf{k})$ are associated with the poles of the resolvent operator $1/[z-L_E(\mathbf{k})]$ or with those M values $z=z_j(k)$ $(j=1,2,\ldots,M)$ for which

$$D(k,z)=\det[\mathbb{1}-\mathscr{A}(k,z)\mathscr{T}(k)]=0. \tag{2.28}$$

The correlation functions $S_{\alpha\beta}(k,\omega)$ are then given by a sum of M Lorentzians:

$$S_{\alpha\beta}(k,\omega)=\frac{1}{\pi}\mathrm{Re}\sum_{j=1}^{M}\frac{M^{(j)}_{\alpha\beta}(k)}{i\omega-z_j(k)}, \tag{2.29}$$

where the $z_j(k)$ are the eigenvalues of $L_E(\mathbf{k})$, and the $M^{(j)}_{\alpha\beta}(k)$, the corresponding amplitudes, are given by

$$M^{(j)}_{\alpha\beta}(k)=\frac{1}{D'(k,z_j)}[\mathscr{T}(k,z_j)\mathscr{A}(k,z_j)]_{\alpha\beta}. \tag{2.30}$$

Here $\mathscr{T}$ is the transpose of the matrix of cofactors of $\mathbb{1}-\mathscr{A}\mathscr{T}$ and $D'(k,z_j)=\{dD(k,z)/dz\}_{z=z_j}$.

In earlier approximations[14,15] we used $M=10$, but all results reported here are based on $M=35$ at least. For $M=35$, the convergence of the eigenmodes relevant for the computation of the $S_{\alpha\beta}$ could be ascertained, which was not possible before for $M=10$.

The discrete eigenvalues of $L_E(\mathbf{k})$ are of two types: real or each other's complex conjugate, but all with negative real parts.[14,23] The first type corresponds to eigenmodes describing diffusive, purely damped processes, while the second type describes propagating (and damped) processes.

Because of the nature of the functions ϕ_j, only longitudinal eigenmodes of $L_E(\mathbf{k})$ (with $\mathbf{v}\|\mathbf{k}$) are obtained here. Of all the eigenvalues of $L_E(\mathbf{k})$, three eigenvalues go to zero when k goes to zero: They reduce to the three hydrodynamic eigenvalues, whose eigenfunctions are linear combinations of ϕ_1, ϕ_2, and ϕ_3, i.e., of the density, longitudinal velocity, and temperature, respectively. The eigenvalues are the same as derived from the Navier-Stokes equations, viz., a heat mode, with eigenvalue

$$z_h(k)=-D_{TE}k^2, \tag{2.31}$$

and two sound modes, with eigenvalues

$$z_\pm(k)=\pm i\omega_s(k)+z_s(k), \tag{2.32}$$

with dispersion

$$\omega_s(k)=ck \tag{2.33}$$

and damping

$$z_s(k)=-\Gamma_E k^2. \tag{2.34}$$

Here c is the adiabatic velocity of sound in the hard-sphere fluid and D_{TE} and Γ_E are the thermal diffusivity and the sound damping coefficients, respectively, as given by the Enskog transport theory.[27]

For $k\to 0$, the $S_{\alpha\beta}(k,\omega)$ are given by the Landau-Placzek expressions[2]

$$S_{\alpha\beta}(k,\omega)=\frac{1}{\pi}\mathrm{Re}\sum_{j=h,\pm}\frac{M_{\alpha\beta}^{(j)}}{i\omega-z_j(k)} \tag{2.35}$$

with $M_{11}^{(h)}=(\gamma-1)/\gamma$, $M_{13}^{(h)}=(\gamma-1)^{1/2}/\gamma$, and $M_{33}^{(h)}=1/\gamma$ for the heat-mode contributions and $M_{11}^{(\pm)}=1/(2\gamma)$, $M_{13}^{(\pm)}=-(\gamma-1)^{1/2}/(2\gamma)$, and $M_{33}^{(\pm)}=(\gamma-1)/(2\gamma)$ for the sound-mode contributions where $\gamma=c_p/c_v$ is the ratio of specific heats at constant pressure (c_p) and constant volume (c_v) for the hard-sphere fluid.

All other eigenvalues of $L_E(\mathbf{k})$ approach finite, negative real values when k goes to zero. They correspond to kinetic eigenmodes of $L_E(\mathbf{k})$ which are for small k irrelevant for the $S_{\alpha\beta}(k,\omega)$, since all $M_{\alpha\beta}^{(j)}(k)$ tend to zero for $k\to 0$ when $j\neq h,\pm$.

The $S_{\alpha\beta}(k,\omega)$ are well approximated by the hydrodynamic Landau-Placzek expressions [i.e., Eqs. (2.29)—(2.35)] for $0\leqq kl_E<0.1$ at low densities, the range diminishing somewhat with increasing density. For $kl_E>0.1$ we have calculated the $S_{\alpha\beta}(k,\omega)$ in two ways, either by using 35 discrete eigenmodes [cf. Eq. (2.29)] or using the matrix inversion [cf. Eqs. (2.24) and (2.27)]. We will show in the next sections that the contributions of the three hydrodynamic modes $j=h,\pm$, extended to $kl_E>0.1$, dominate the $S_{\alpha\beta}(k,\omega)$ up to $kl_E\approx 1$ for most densities. This enables us to analyze the behavior of the correlation function in terms of dynamic processes that are generalizations of those from Navier-Stokes hydrodynamics.

III. DILUTE GASES

A. Boltzmann theory

For low densities, i.e., $V_0/V=n\sigma^3/\sqrt{2}<0.1$ and sufficiently small k, such that $k\sigma\ll 1$, but $kl_0\approx O(1)$ and not necessarily small, the eigenmodes of $L_E(\mathbf{k})$ approach those of the inhomogeneous linear Boltzmann operator[17]

$$L_E(\mathbf{k})\underset{\substack{n\sigma^3<0.1,\\ k\sigma\ll 1}}{\longrightarrow}L_B(\mathbf{k})=-i\mathbf{k}\cdot\mathbf{v}+n\Lambda_B\ , \tag{3.1}$$

with

$$\Lambda_B h(\mathbf{v}_1)=-\sigma\int d\hat{\sigma}\int d\mathbf{v}_2\,\phi(v_2)\theta(\mathbf{v}_{12}\cdot\hat{\sigma})\,|\,\mathbf{v}_{12}\cdot\hat{\sigma}\,|\,[h(\mathbf{v}_1)+h(\mathbf{v}_2)-h(\mathbf{v}_1')-h(\mathbf{v}_2')]\ , \tag{3.2}$$

since then $\chi\to 1$, $\overline{A}_{\mathbf{k}}\to 0$, $\Lambda_{\mathbf{k}}\to\Lambda_B$, and $\langle\Lambda_B h(\mathbf{v}_1)\rangle_1=0$. Although one could consider the case $k\sigma\approx O(1)$, corresponding to neutron scattering, the practically relevant case is that of $kl_0\approx 0(1)$ and $k\sigma\approx 0$, corresponding to light scattering of dilute gases.

B. Boltzmann eigenmodes

The first 12 eigenvalues of $L_B(\mathbf{k})$ in the BGK approximation $M=35$ are plotted in Fig. 1 as a function of kl_0 for $kl_0\leqq 1$. For $0<kl_0<0.1$, the hydrodynamic eigenvalues of $L_B(\mathbf{k})$ are given by the Eqs. (2.31)—(2.34), where c, D_{TE}, and Γ_E reduce to their values for a dilute gas of hard spheres.

The striking feature is that the extensions of the real parts of the heat- and the sound-mode eigenvalues remain well separated from the real parts of all the kinetic eigenvalues as long as $kl_0\leqq 1$. Thus, even up until kl_0 in the neighborhood of 1, the correlation functions will still be dominated by the three (extended) hydrodynamic modes, since these modes damp out much more slowly than the kinetic modes. Indeed, the contributions of the three extended hydrodynamic modes to S_{11} and S_{13} are indistinguishable from the "exact" values of these functions, obtained with $M=35$ by matrix inversion, up to $kl_0\approx 0.4$ and approximate them very well up to $kl_0\approx 0.8$, as shown in Fig. 2. Even at $kl_0\approx 1$, the three modes still account for about 75% of the contributions (cf. Fig. 2).

The representation of S_{33} in terms of three extended hydrodynamic modes is less satisfactory and differences appear already at $kl_0=0.3$ (cf. Fig. 2). The reason for

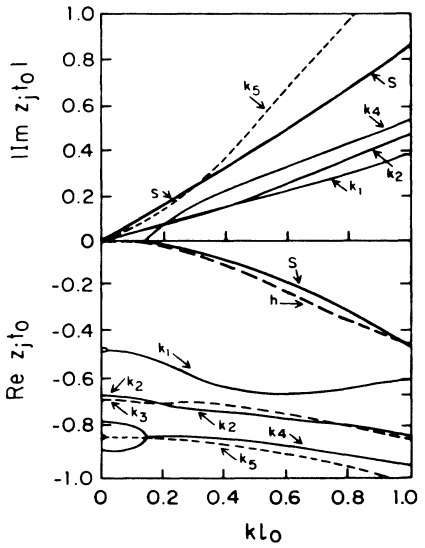

FIG. 1. Reduced real and absolute value of imaginary part of the 12 highest eigenvalues of the hard-sphere Boltzmann operator from BGK with $M=35$, as a function of the reduced wave number: three hydrodynamic (h,s) and nine kinetic (k) modes and their extensions. The heat mode h and the kinetic mode k_3 are real (damped) for all k; the sound modes s are complex (propagating and damped) for all k. The remaining eight kinetic modes start as two (almost degenerate) real modes, which become complex for larger kl_0. Note that eigenvalues of a pair of propagating modes have the same real parts and the same absolute values (but opposite signs) of their imaginary parts. l_0 and t_0 are the Boltzmann mean free path and time, respectively.

this is that temperature fluctuations couple much more strongly than density fluctuations to kinetic eigenmodes. A better representation of S_{33} will be discussed later (see Sec. VI, subparagraph 2). The dominance of the extended hydrodynamic modes implies that the collisional invariants remain important far beyond the hydrodynamic regime. The value $kl_0 \approx 0.8$ corresponds to $\lambda \approx 8l_0$, i.e., eight collisions within a wavelength. This number is consistent with Erpenbeck's observation that in molecular-dynamics simulations of hard-sphere fluids approximately eight collisions are needed to obtain local equilibrium, i.e., to obtain a hydrodynamiclike description.[28]

C. Matrix inversion

For $kl_0 \geqq 1$ all the eigenvalues mix in a complicated manner and a description of the correlation functions in terms of collective modes, i.e., three hydrodynamiclike modes only, becomes impossible. In fact, matrix inversion has to be used to describe the $S_{\alpha\beta}(k,\omega)$. Therefore, a simplified description of the $S_{\alpha\beta}(k,\omega)$ in terms of only a few eigenmodes of $L_E(\mathbf{k})$, which are the extensions of those at small k, does not exist anymore.

D. Ideal gas and single binary collisions

However, for $kl_0 \geqq 50$, an individual-particle description is possible, in that the operator $L_B(\mathbf{k})$ effectively reduces to its free-streaming part $-i\mathbf{k}\cdot\mathbf{v}$ and the correlation functions are given by their ideal gas values.[18]

Corrections to this behavior can be obtained by an expansion of the resolvent operator $1/[z-L_E(\mathbf{k})] = 1/[z-L_B(\mathbf{k})]$ around free streaming, which leads to an expansion in sequences of binary collisions, characterized by Λ_B, i.e.,[17,29]

$$\frac{1}{z-L_B(\mathbf{k})} = \frac{1}{z+i\mathbf{k}\cdot\mathbf{v}-n\Lambda_B} = \frac{1}{z+i\mathbf{k}\cdot\mathbf{v}} + \frac{1}{z+i\mathbf{k}\cdot\mathbf{v}} n\Lambda_B \frac{1}{z+i\mathbf{k}\cdot\mathbf{v}} + \cdots , \tag{3.3}$$

where the first term in the expansion on the right-hand side of Eq. (3.3) is the ideal-gas contribution and the second term

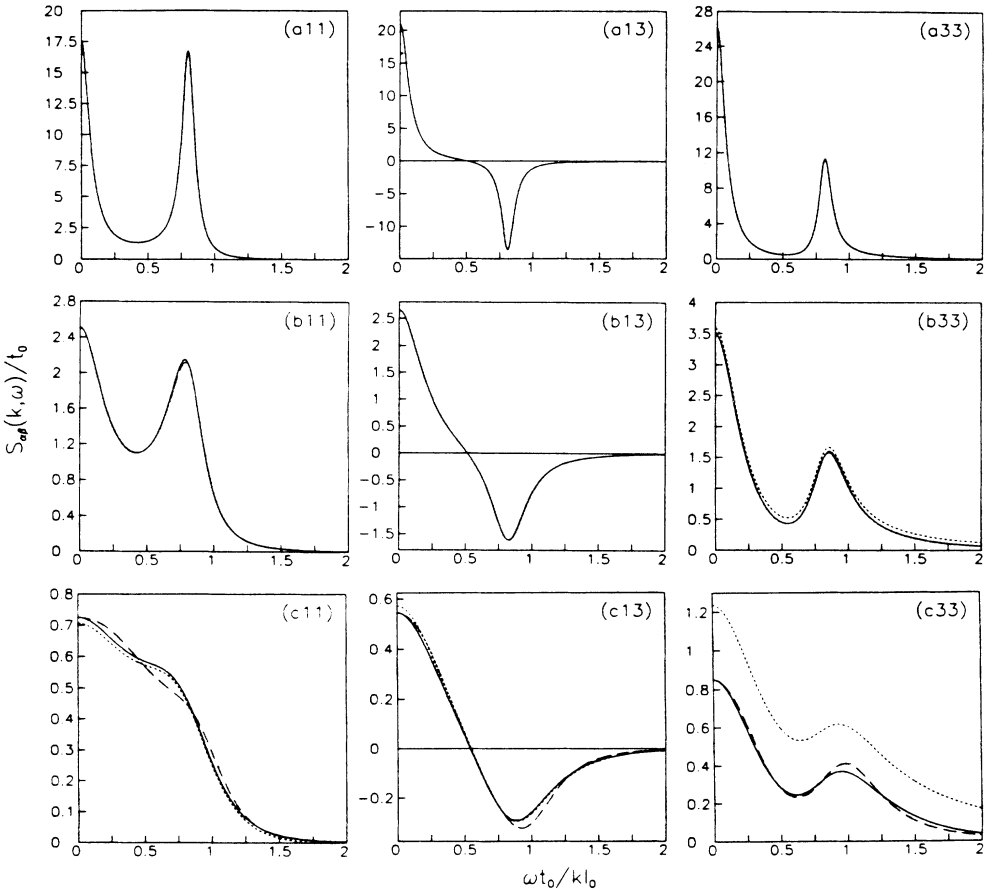

FIG. 2. Dilute-gas correlation functions $S_{\alpha\beta}(k,\omega)/t_0$ as a function of $\omega t_0/kl_0$ for selected values of kl_0. The letters refer to the values of kl_0: (a) $=kl_0=0.1$; (b) $=kl_0=0.3$; (c) $=kl_0=0.8$ and pairs of numbers (11), (13), (33) to the values of $\alpha\beta$. —— denotes $S_{\alpha\beta}$ computed from BGK by matrix inversion with $M=35$; · · · ·, with three extended hydrodynamic modes; and — — —, with five effective modes.

the contribution of a single binary collision. From this, one finds for the $S_{\alpha\beta}(k,\omega)$ an expansion in powers of $1/kl_0$ with coefficients that depend on the reduced frequency $\omega^*=\omega t_0/kl_0=(\pi m/8k_BT)^{1/2}\omega/k$, i.e.,

$$S_{11}(k,\omega)=\frac{2}{\pi}\frac{t_0}{kl_0}\left[e^{-(4/\pi)(\omega^*)^2}+\frac{s_{11}^B(\omega^*)}{kl_0}+O(1/(kl_0)^2)\right],$$
$$S_{13}(k,\omega)=\frac{1}{\pi}\left[\frac{2}{3}\right]^{1/2}\frac{t_0}{kl_0}\left[e^{-(4/\pi)(\omega^*)^2}\left[1-\frac{8}{\pi}(\omega^*)^2\right]+\frac{s_{13}^B(\omega^*)}{kl_0}+O(1/(kl_0)^2)\right], \tag{3.4}$$
$$S_{33}(k,\omega)=\frac{5}{3\pi}\frac{t_0}{kl_0}\left[e^{-(4/\pi)(\omega^*)^2}\left[1-\frac{16}{5\pi}(\omega^*)^2+\frac{64}{5\pi^2}(\omega^*)^4\right]+\frac{s_{33}^B(\omega^*)}{kl_0}+O(1/(kl_0)^2)\right].$$

Here the leading terms are the ideal-gas contributions and the terms containing the $s_{\alpha\beta}^B(\omega^*)$ are the corrections to the ideal-gas contributions due to a single binary collision. We have calculated the $s_{\alpha\beta}^B(\omega^*)$ numerically using the BGK method with M up to 50. The $s_{\alpha\beta}^B(\omega^*)$ are shown in Fig. 3 as functions of ω^*. We note that $s_{11}^B(\omega^*)$ agrees very well with the analytical evaluation of the single-collision term (Ref. 29).

Remarkably, the single-collision terms in Eq. (3.4) give corrections to ideal-gas behavior, sufficient to describe the $S_{\alpha\beta}$ for all $3<kl_0<\infty$ (cf. Fig. 4). Therefore, with the exception of the region $1<kl_0<3$, a simplified description of the correlation functions in terms of either collective or individual-particle modes of the fluid is possible and an identification of the relevant dynamical processes can be made.

The results for S_{11}, i.e., $S(k,\omega)$, agree well with those obtained experimentally by Clark[1] for a dilute Xe gas for $0<kl_0\leqq 6$, i.e., for $0<kl_0<1$ the three (extended) hydrodynamic modes describe the experimental $S(k,\omega)$, while for $3<kl_0\leqq 6$, the ideal gas plus one binary collision suffices.

IV. DENSE FLUIDS

A. True eigenmodes

For fluids at high densities, i.e. $0.35<V_0/V<0.70$, the eigenmodes of $L_E(\mathbf{k})$ behave quite differently from those of dilute gases. Indeed, of the three extended hydrodynamic eigenvalues only the heat-mode eigenvalue stays separate from those of the other (hydrodynamic and kinetic) eigenmodes, when kl_E increases from the hydrodynamic regime, $0\leqq kl_E<0.05$, to $kl_E\approx 1$. This separation increases with increasing density and, in addition, an increasingly pronounced maximum around $k\sigma\approx 2\pi$ in the heat-mode eigenvalue develops. The extended sound modes, however, mix already with kinetic modes at $k\sigma\approx 2.5$, i.e., long before $kl_E\approx 1$. To illustrate this, we show in Fig. 5(a) the highest-lying BGK eigenvalues of $L_E(\mathbf{k})$ for $M=35$, as functions of $k\sigma$ for $0\leqq k\sigma<10$ at $V_0/V=0.625$, where $\sigma/l_E=19.5$, so that $k\sigma=2.5$ corresponds to $kl_E=0.13$. We see that the heat-mode eigenvalue $z_h(k)$ is well separated from all other eigenvalues but that the sound damping $z_s(k)$ mixes with the kinetic modes for $k\sigma>2.5$. In addition, all kinetic modes mix with each other in a very complicated fashion, which changes with M in a seemingly arbitrary and certainly nonconvergent way. This can be seen in Fig. 5(b) where the highest BGK eigenvalues are also plotted for $M=55$. Therefore, no significance can be given to each single eigenmode of $L_E(\mathbf{k})$ as obtained by the $M=35$ BGK approximation for $k\sigma\geqq 2.5$, except to the heat mode which is the same for $M=35$ and 55 (cf. Fig. 5).

Thus a simple Landau-Placzek-like picture where the $S_{\alpha\beta}(k,\omega)$ can be described by three extended hydrodynamic modes up to $kl_E\leqq 1$ does not obtain. This observation is contrary to that of previous calculations,[15] using a BGK approximation of $M=10$, and is a consequence of a more complete analysis of the eigenmodes of $L_E(\mathbf{k})$ using $M=35$ or even $M=55$. We should note, however, that at each value of $kl_E<1$ and for $M\geqq 10$, the $S_{\alpha\beta}(k,\omega)$ computed by using the heat mode and only a few of the highest-lying kinetic modes are very insensitive

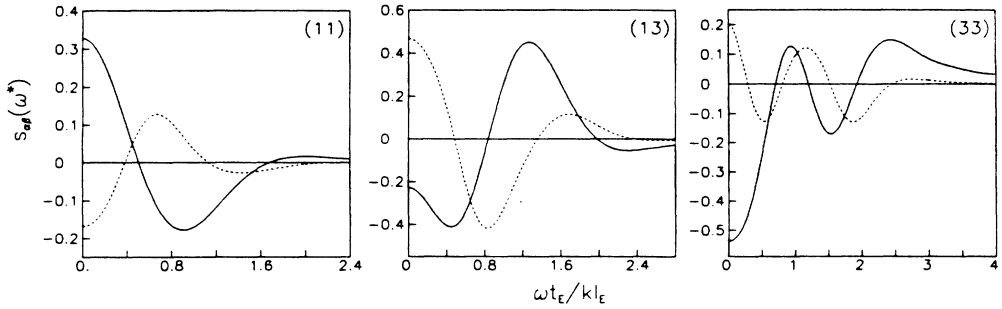

FIG. 3. First binary collision correction of the $s_{\alpha\beta}$ ($\alpha\beta=11,13,33$) to the ideal-gas limit as a function of $\omega^*=\omega t_0/kl_0=\omega t_E/kl_E$ from the hard-sphere Boltzmann $s_{\alpha\beta}^B(\omega^*)$ (· · · ·) and the Lorentz-Boltzmann $s_{\alpha\beta}^{LB}(\omega^*)$ (——) equations.

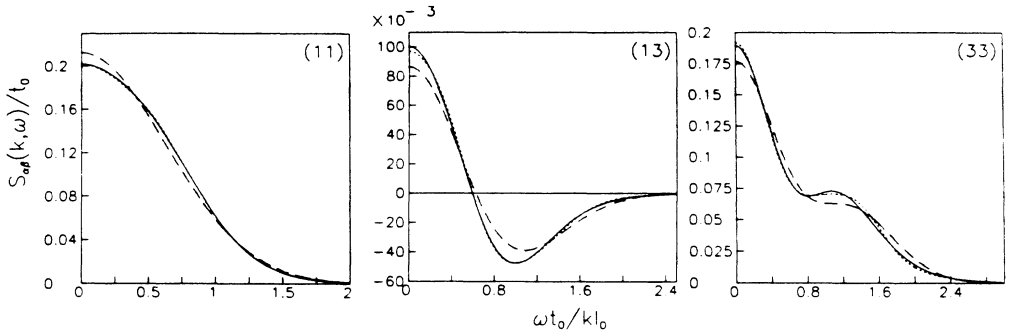

FIG. 4. Dilute hard-sphere gas correlation functions $S_{\alpha\beta}(k,\omega)/t_0$ (——) for $\alpha\beta=11,13,33$ as a function of $\omega t_0/kl_0$ for $kl_0=3$. Also plotted are the ideal gas limit (— — —) and this limit plus the first binary collision correction (from the Boltzmann equation) (· · · ·), which is for almost all ω indistinguishable from $S_{\alpha\beta}(k,\omega)$.

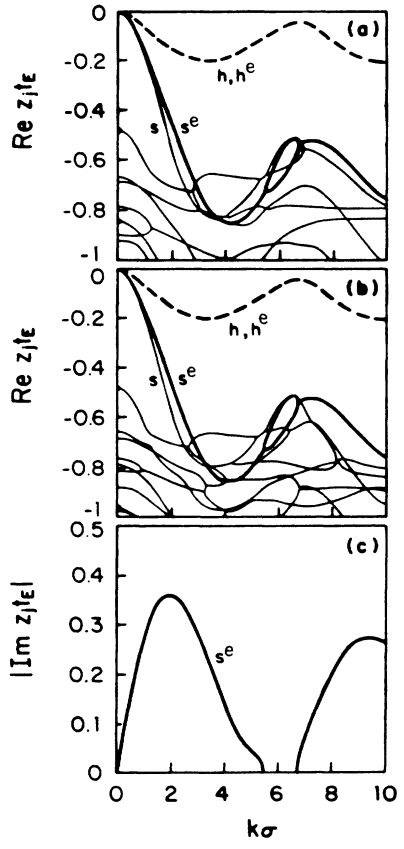

FIG. 5. Reduced eigenvalues of the Enskog operator for a dense hard-sphere gas at $V_0/V=0.625$ as a function of the reduced wave number $k\sigma$. (a) Real part of highest eigenvalues from BGK with $M=35$ (thin solid curves) and three effective heat and sound modes (thick solid curves), where the effective heat mode (at the top) is indistinguishable from that of BGK with $M=35$; (b) same as in (a) with $M=55$; (c) absolute value of imaginary parts of the two effective sound modes. Note in (c) a propagation gap around $k\sigma\approx 6$ and in (a) and (b) an excellent convergence of effective modes but lack of convergence of other modes, except the heat mode (— — —).

to M, i.e., to the detailed behavior of the individual eigenmodes, and describe the exact $S_{\alpha\beta}(k,\omega)$ very well, in spite of the slow convergence of the individual modes.

B. Effective eigenmodes

Yet, a simple Landau-Placzek-like description of the $S_{\alpha\beta}(k,\omega)$ still obtains for all $kl_E<1$, if the joint contributions of the highest-lying "true" eigenmodes of $L_E(\mathbf{k})$ are approximated by the eigenmodes of an effective 3×3 matrix $\underline{H}^e(k)$—the effective modes—which replaces effectively the $\infty\times\infty$ matrix $\mathscr{L}^E(k)$ as a description of the dominant dynamical processes of the fluid. We start with deriving $\underline{H}^e(k)$ from $\mathscr{L}^E(k)$ in order to clarify the physical nature of the approximation.

(a) The 3×3 matrix $\underline{H}^e(k)$ is obtained from a contraction of the ∞ set of generalized hydrodynamic equations for the $\mathscr{G}_{jl}(k,z)=\langle\phi_j(\mathbf{v}_1)[z-L_E(\mathbf{k})]^{-1}\phi_l(\mathbf{v}_1)\rangle_1$:

$$z\mathscr{G}_{jl}(k,z)=\sum_{i=1}^{\infty}\mathscr{L}^E_{ji}(k)\mathscr{G}_{il}(k,z)+\delta_{jl} \tag{4.1}$$

to a set of three equations in the following way. For each fixed $l=\beta=1,2,3$ the $\mathscr{G}_{i\beta}(k,z)$ with $i>3$ can be eliminated from the first three equations with $j=\alpha=1,2,3$, by solving successively the equations for $\mathscr{G}_{j\beta}(k,z)$ with $j>3$ for $\mathscr{G}_{j\beta}(k,z)$ $(j>3)$ in terms of the $\mathscr{G}_{j\beta}(k,z)$ with $j\leqq 3$. Then one obtains a 3×3 matrix equation for the $G_{\alpha\beta}(kz)$ $(\alpha,\beta=1,2,3)$ alone, i.e., the generalized hydrodynamiclike equation

$$zG_{\alpha\beta}(k,z)=\sum_{\gamma=1}^{3}H_{\alpha\gamma}(k,z)G_{\gamma\beta}(k,z)+\delta_{\alpha\beta}\ , \tag{4.2}$$

with

$$H_{\alpha\beta}(k,z)=\mathscr{L}^E_{\alpha\beta}(k)+\Delta\mathscr{L}^E_{\alpha\beta}(k,z)\ . \tag{4.3}$$

Here $\Delta\mathscr{L}^E_{\alpha\beta}(k,z)$ results from the elimination procedure and depends therefore on the $\mathscr{L}^E_{jl}(k)$ with $j,l>3$ and on z, through the z on the left-hand sides of the equations (4.1) with $j>3$. Finally, the $G_{\alpha\beta}(k,z)$ are approximated by the $G^e_{\alpha\beta}(k,z)$ which follow from the simpler generalized hydrodynamiclike equation,

$$zG^e_{\alpha\beta}(k,z)=\sum_{\gamma=1}^{3} H^e_{\alpha\gamma}(k)G^e_{\gamma\beta}(k,z)+\delta_{\alpha\beta} \tag{4.4}$$

with

$$H^e_{\alpha\beta}(k)=H_{\alpha\beta}(k,0)=\mathscr{L}^E_{\alpha\beta}(k)+\Delta\mathscr{L}^E_{\alpha\beta}(k,0)\ . \tag{4.5}$$

Thus the $G^e_{\alpha\beta}(k,z)$ will be good approximations to the $G_{\alpha\beta}(k,z)$ when the z dependence of the $\Delta\mathscr{L}^E_{\alpha\beta}(k,z)$ can be neglected, so that $H_{\alpha\beta}(k,z)\approx H_{\alpha\beta}(k,0)=H^e_{\alpha\beta}(k)$. Equivalently, Eq. (4.4) follows from Eq. (4.1) when, in the elimination procedure, one sets $z=0$ on the left-hand side of all equations with $j>3$. Physically, this means that it is assumed that the time decay of any

$$F^E_{jl}(k,t)=\langle\phi_j(\mathbf{v}_1)\exp[tL_E(\mathbf{k})]\phi_l(\mathbf{v}_1)\rangle_1$$

with $j,l>3$ is much faster than that of any $F^E_{\alpha\beta}(k,t)$ with $\alpha,\beta=1,2,3$.

(b) In practice it is extremely simple to determine $\underline{H}^e(k)$ from $\mathscr{L}^E(k)$. In fact, it is even easier than the matrix inversion mentioned above, since one only has to use Eq. (4.2) with $z=0$ and Eq. (4.5), so that

$$\underline{H}^e(k)=-[\underline{G}(k,0)]^{-1}\ , \tag{4.6}$$

where the 3×3 matrix $\underline{G}(k,0)$ is obtained from the BGK method with $M=35$ or 55 [cf. Eq. (2.24)].

(c) Since [cf. Eq. (4.4)],

$$G^e_{\alpha\beta}(k,z)=\left[\frac{1}{z\mathbb{1}-\underline{H}^e(k)}\right]_{\alpha\beta}\ , \tag{4.7}$$

the $S^e_{\alpha\beta}(k,\omega)$ computed with the 3×3 effective matrix are given by

$$S^e_{\alpha\beta}(k,\omega)=\frac{1}{\pi}\mathrm{Re}\left[\frac{1}{i\omega\mathbb{1}-\underline{H}^e(k)}\right]_{\alpha\beta}\ , \tag{4.8}$$

or equivalently by

$$S^e_{\alpha\beta}(k,\omega)=\frac{1}{\pi}\mathrm{Re}\sum_{j=h,\pm}\frac{M^{e(j)}_{\alpha\beta}(k)}{i\omega-z^e_j(k)}\ , \tag{4.9}$$

where the $M^{e(j)}_{\alpha\beta}(k)$ and $z^e_j(k)$ are found for all k from the eigenmodes of $\underline{H}^e(k)$, which we call "effective" eigenmodes. In Fig. 5, the three effective eigenvalues of $\underline{H}^e(k)$ are compared with the true eigenvalues, i.e., the eigenvalues determined by Eq. (2.28), for $V_0/V=0.625$. We note the following properties of the effective modes.

(1) The effective eigenvalues of $\underline{H}^e(k)$ reduce for small k to those of the Navier-Stokes equations. The effective eigenfunctions are linear combinations of ϕ_1, ϕ_2, and ϕ_3. In particular, the $z^e_j(k)$ and $M^{e(j)}_{\alpha\beta}(k)$ reduce to the expressions given by the Eqs. (2.31)—(2.35). Thus the effective hydrodynamic modes are also extensions of the usual hydrodynamic modes to larger values of k.

(2) Unlike the true extended hydrodynamic eigenmodes, the effective modes are very stable as M increases and do not change significantly for $M\geqq5$, and in particular do not change from $M=35$ to 55 (cf. Fig. 5).

(3) With increasing density, the effective heat mode increasingly coincides with the true heat mode. (Cf. Fig. 5, where the two are indistinguishable for $V_0/V=0.625$.)

(4) The behavior of the effective sound modes obtained here for $M=35$ or 55 is very similar to that determined before for the "true" sound modes[15] for $M=10$. In particular, a gap in $\omega_s(k)$ is present near $k\sigma=2\pi$ at high densities (cf. Fig. 5). A detailed discussion of the extended hydrodynamic eigenmodes and the physical origin of their behavior has been given before.[15,30]

C. Effective mode description

The three effective modes can be used to evaluate all the correlation functions $S^e_{\alpha\beta}(k,\omega)$, using the Landau-Placzek-like formula, Eq. (4.9). In Fig. 6, the $S^e_{\alpha\beta}(k,\omega)$ are compared with their "exact" Enskog values $S_{\alpha\beta}(k,\omega)$ computed with $M=35$ and using matrix inversion [cf. Eqs. (2.24) and (2.27)] for selected values of k at $V_0/V=0.625$.

We note that the $S^e_{\alpha\beta}(k,\omega)$ computed with the effective modes obey the following sum rules:

$$S^e_{\alpha\beta}(k,\omega=0)=S_{\alpha\beta}(k,\omega=0)\ , \tag{4.10}$$

$$\int_0^\infty d\omega\, S^e_{\alpha\beta}(k,\omega)=\int_0^\infty d\omega\, S_{\alpha\beta}(k,\omega)\ , \tag{4.11}$$

and

$$\int_0^\infty d\omega\,\omega^2 S^e_{11}(k,\omega)=\int_0^\infty d\omega\,\omega^2 S_{11}(k,\omega)=\frac{k_BT}{2mS(k)}k^2\ . \tag{4.12}$$

As a result of these sum rules, the $S^e_{\alpha\beta}(k,\omega)$ [and in particular $S^e_{11}(k,\omega)$] never differ too much from the $S_{\alpha\beta}(k,\omega)$, contrary to the $S_{\alpha\beta}(k,\omega)$ computed with the true eigenmodes, as is illustrated for the case of $S_{33}(k,\omega)$ for a dilute gas in Fig. 2, (c33).

That the three effective modes of $\underline{H}^e(k)$ describe the correlation functions of a dense hard-sphere fluid so well for $0<kl_E<1$ (cf. Fig. 6) is due to

(1) the dominance of the matrix elements $\mathscr{L}^E_{\alpha\beta}(k)$ with $\alpha,\beta=1,2,3$ over $\Delta\mathscr{L}^E_{\alpha\beta}(k,0)$ in $\underline{H}^e(k)$,

(2) the dominance of the extended heat mode, which remains virtually unchanged when we go from $L_E(\mathbf{k})$ to $\underline{H}^e(k)$, and

(3) the dominance of only a few of the highest-lying (intersecting) true kinetic modes of $L_E(\mathbf{k})$ which are apparently well represented by the two effective sound modes of $\underline{H}^e(k)$.

We note the close resemblance of the eigenvalues of the three effective modes to those obtained with $M=10$ (or even $M=3$).[15,31] In particular both exhibit a pronounced maximum of the heat-mode eigenvalue as well as a propagation gap in the sound dispersion curve.[14,15]

Therefore, the dynamical processes that take place in the fluid on the molecular scale and that are relevant for the hydrodynamic correlation functions can be represented for high densities by three effective hydrodynamiclike modes: a heat mode and two soundlike modes.

D. Ideal gas and single binary collisions

For $kl_E\geqq1$, the three effective hydrodynamic modes lose their significance and the correlation functions $S_{\alpha\beta}$ can most easily be obtained by matrix inversion. However, as in the case of a dilute gas, for $kl_E>50$, an individual-particle description is applicable, leading to

ideal-gas-like behavior of the correlation functions.

In addition, as in the case of a dilute gas, for $kl_E \gg 1$, the resolvent operator $1/[z-L_E(\mathbf{k})]$ can be expanded around the ideal-gas behavior, which is now characterized by the Lorentz-Boltzmann operator[14] $\Lambda^s=\lim_{k\to\infty}\Lambda_{\mathbf{k}}$ instead of by Λ_B. Including only the first two terms in this expansion, i.e., the ideal-gas contribution and a single binary collision, leads to

$$S_{11}(k,\omega)=\frac{2}{\pi}\frac{t_E}{kl_E}\left[e^{-(4/\pi)(\omega^*)^2}+\frac{s_{11}^{LB}(\omega^*)}{kl_E}+O(1/(kl_E)^2)\right],$$

$$S_{13}(k,\omega)=\frac{1}{\pi}\left[\frac{2}{3}\right]^{1/2}\frac{t_E}{kl_E}\left[e^{-(4/\pi)(\omega^*)^2}\left[1-\frac{8}{\pi}(\omega^*)^2\right]+\frac{s_{13}^{LB}(\omega^*)}{kl_E}+O(1/(kl_E)^2)\right],$$

$$S_{33}(k,\omega)=\frac{5}{3\pi}\frac{t_E}{kl_E}\left[e^{-(4/\pi)(\omega^*)^2}\left[1-\frac{16}{5\pi}(\omega^*)^2+\frac{64}{5\pi^2}(\omega^*)^4\right]+\frac{s_{33}^{LB}(\omega^*)}{kl_E}+O(1/(kl_E)^2)\right], \tag{4.13}$$

with

$$\omega^*=\omega t_E/kl_E=(\pi m/8k_BT)^{1/2}\omega/k\ ,$$

as in Eq. (3.4). We note that $t_E/l_E=t_0/l_0$ for all densities so that the ideal-gas terms in Eqs. (3.4) and (4.13) are the same. The functions $s_{\alpha\beta}^{LB}(\omega^*)$, which determine the single-binary-collision terms in Eq. (4.13), are calculated numerically in a fashion similar to that discussed for low densities[17,29] and the results are shown in Fig. 3. The function $s_{11}^{LB}(\omega^*)$ is in very good agreement with the analytical evaluation of $s_{11}^{LB}(\omega^*)$ given in Ref. 32.

We find that the $S_{\alpha\beta}(k,\omega)$ at high densities are well described by Eq. (4.13) for $3<kl_E<\infty$ (cf. Fig. 7). Thus,

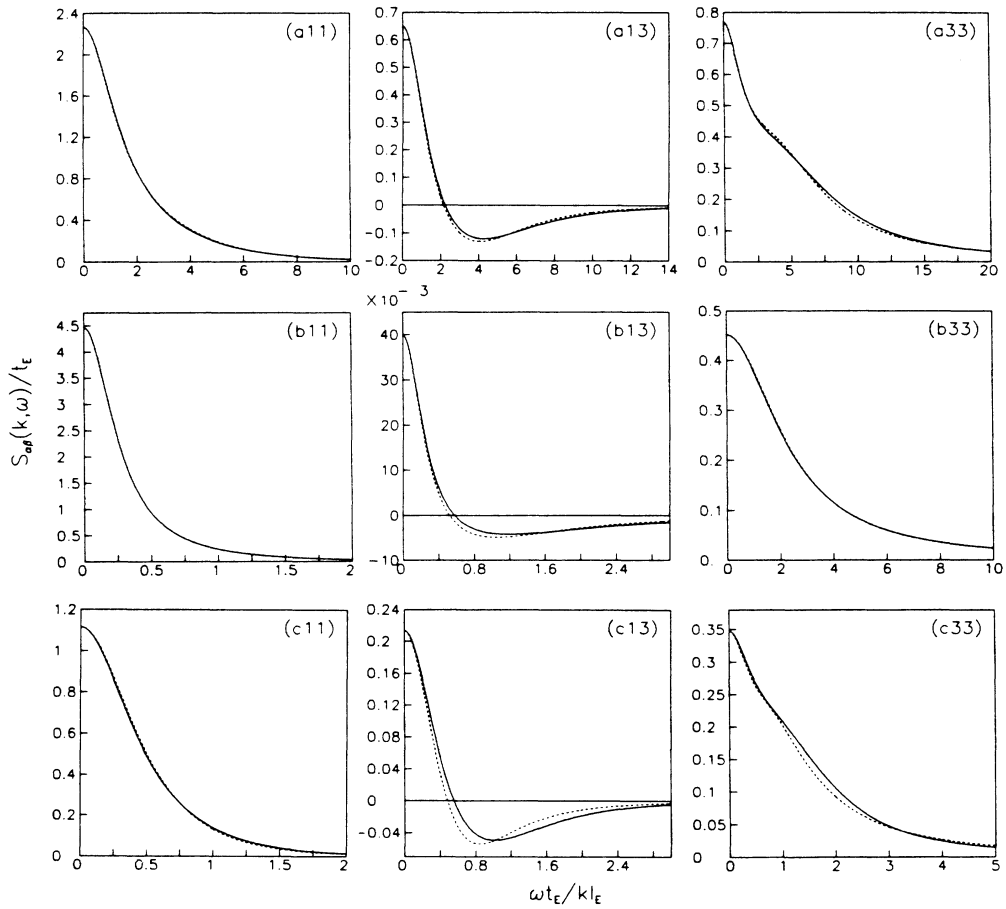

FIG. 6. Dense hard-sphere fluid, $V_0/V=0.625$, correlation functions $S_{\alpha\beta}(k,\omega)/t_E$ as a function of $\omega t_E/kl_E$ for selected values of kl_E. The letters and numbers labeling the figures are as in Fig. 2 (with l_0,t_0 replaced by l_E,t_E). ——, from BGK matrix inversion with $M=35$; · · · ·, from three effective modes. l_E and t_E are the Enskog mean free path and time, respectively.

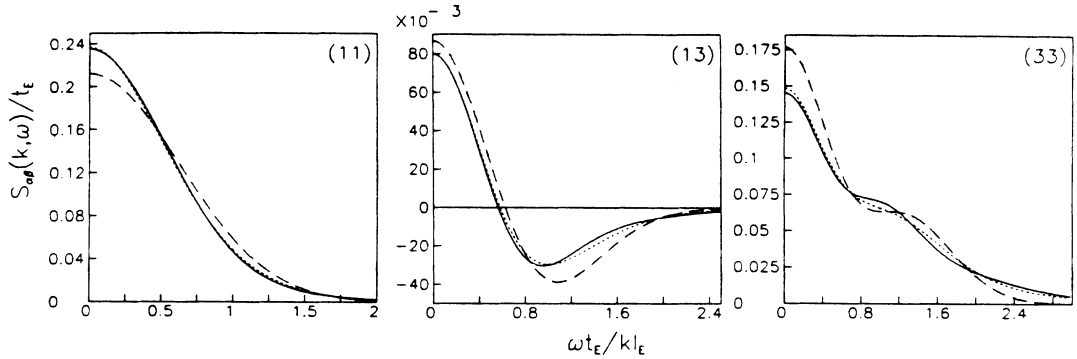

FIG. 7. Dense hard-sphere fluid, $V_0/V=0.625$, correlation functions $S_{\alpha\beta}(k,\omega)/t_E$ obtained from BGK with $M=35$ (——) as a function of $\omega t_E/kl_E$ for $kl_E=3$. Also plotted are the ideal-gas limits (— — —) and this limit plus the first binary collision correction (from the Lorentz-Boltzmann equation) (· · · ·), which is indistinguishable from $S_{\alpha\beta}(k,\omega)$ for most ω.

as for low densities, for $kl_E>3$ the behavior of the correlation functions can be understood on the basis of free streaming of the particles and a single-binary-collision process. However, since the $s^B_{\alpha\beta}(\omega^*)$ are markedly different from the $s^{LB}_{\alpha\beta}(\omega^*)$ (cf. Fig. 3), the approach to ideal-gas behavior for low densities, described by Λ_B, is markedly different from that at high densities, described by Λ^s. This is related[29] to the fact that Λ_B has five collisional invariants, while Λ^s has only one.

V. INTERMEDIATE DENSITIES

A. Three modes

For fluids at intermediate densities $0.1<V_0/V<0.35$, a simple Landau-Placzek-like description of the hydrodynamic correlation functions, with either three true or three effective extended hydrodynamic modes does not seem possible beyond the Navier-Stokes regime. For, in this intermediate-density regime (unlike in a dilute gas) the extended heat- and sound-mode eigenvalues are not well separated from the kinetic eigenvalues and (unlike in dense fluids) the extended heat-mode eigenvalue is not well separated from those of the other modes.

B. Five modes

One can, however, describe the correlation functions, in this transition regime with five effective modes rather than with the three effective hydrodynamic modes defined in Sec. IV. These five effective modes are obtained in a way similar to that of Sec. IV.

Thereto we consider the 5×5 matrix $\underline{\overline{G}}(k,z)$ of correlation functions $\overline{G}_{\alpha'\beta'}(k,z)$ given by Eq. (2.23) with α' or $\beta'=1,2,\ldots,5$ which include the correlation functions $G_{\alpha\beta}(k,z)$ with $\alpha,\beta=1,2,3$ and in addition α' or $\beta'=4$ [involving $\phi_4(\mathbf{v})$] and α' or $\beta'=5$ [involving $\phi_5(\mathbf{v})$, cf. Eq. (2.17)]. The bar indicates a 5×5 instead of a 3×3 matrix.

All 25 $\overline{G}_{\alpha'\beta'}(k,z)$ can be calculated by matrix inversion using Eq. (2.24) in the BGK approximation with $M=35$, or by approximating them by 25 $\overline{G}^{\,e}_{\alpha'\beta'}(k,z)$, which satisfy the 5×5 matrix equation [cf. Eq. (4.4)]:

$$z\overline{G}^{\,e}_{\alpha'\beta'}(k,z)=\sum_{\gamma'=1}^{5}\overline{H}^{\,e}_{\alpha'\gamma'}(k)\overline{G}^{\,e}_{\gamma'\beta'}(k,z)+\delta_{\alpha'\beta'}\ , \tag{5.1}$$

where the effective 5×5 matrix $\underline{\overline{H}}^{\,e}(k)$ with elements $\overline{H}^{\,e}_{\alpha'\beta'}(k)$ is given by the inverse of the 5×5 matrix $\underline{\overline{G}}(k,0)$:

$$\underline{\overline{H}}^{\,e}(k)=-[\underline{\overline{G}}(k,0)]^{-1}\ . \tag{5.2}$$

One can show that of the five eigenmodes of $\underline{\overline{H}}^{\,e}(k)$, three are extensions of the heat and sound modes in hydrodynamics and two are extensions of kinetic modes that have finite negative eigenvalues when $k\to0$. The eigenfunctions are linear combinations of $\phi_1,\ldots,\phi_5$, i.e., of the density, longitudinal velocity, temperature, stress tensor and heat flux, respectively [cf. Eq. (2.17)]. The $S_{\alpha\beta}(k,\omega)$ in the 5×5 effective mode approximation $\overline{S}^{\,e}_{\alpha\beta}(k,\omega)$ are given by

$$\overline{S}^{\,e}_{\alpha\beta}(k,\omega)=\frac{1}{\pi}\mathrm{Re}\left[\frac{1}{i\omega\mathbb{1}-\underline{\overline{H}}^{\,e}(k)}\right]_{\alpha\beta}=\frac{1}{\pi}\mathrm{Re}\sum_{j=1}^{5}\frac{\overline{M}^{\,e(j)}_{\alpha\beta}(k)}{i\omega-\overline{z}^{\,e}_{j}(k)}\ , \tag{5.3}$$

where the $\overline{M}^{\,e(j)}_{\alpha\beta}(k)$ and $\overline{z}^{\,e}_{j}(k)$ with $j=1,2,\ldots,5$ are for all k obtained from the five effective eigenmodes of $\underline{\overline{H}}^{\,e}(k)$.

Thus, the $\overline{S}^{\,e}_{\alpha\beta}(k,\omega)$ are again represented in a Landau-Placzek-like fashion in terms of the three extended hydrodynamic modes of $\underline{\overline{H}}^{\,e}(k)$ and two extended kinetic modes. Or, equivalently, if a contraction to a 3×3 matrix is made, by three extended hydrodynamic modes with viscoelasticity, i.e., ω-dependent transport coefficients.[33,34]

C. Five-mode description

In Fig. 8 we show the five eigenvalues of $\underline{\overline{H}}^{\,e}(k)$ for $V_0/V=0.25$ and $0\leqq kl_E\leqq1$. In Fig. 9 we compare for the intermediate density $V_0/V=0.25$ and $0\leqq kl_E\leqq1$ the $\overline{S}^{\,e}_{\alpha\beta}(k,\omega)$ with the $S_{\alpha\beta}(k,\omega)$ obtained by matrix inversion. We see that the $\overline{S}^{\,e}_{\alpha\beta}(k,\omega)$ with five effective modes represent the $S_{\alpha\beta}(k,\omega)$ very well. We also plot in Fig. 9 the $S^e_{\alpha\beta}(k,\omega)$ with three effective modes [cf. Eqs. (4.4)—(4.9)] to illustrate that at this density three effective modes give an insufficient description of the $S_{\alpha\beta}(k,\omega)$.

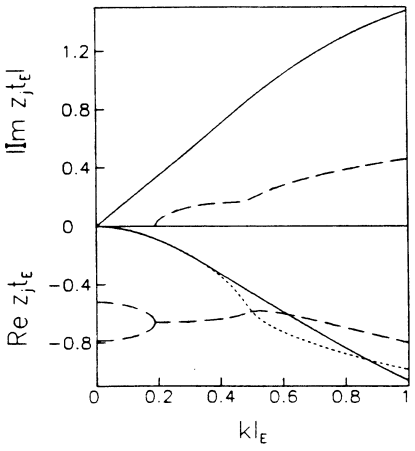

FIG. 8. Reduced real and absolute value of imaginary part of the five effective eigenvalues of the Enskog operator at an intermediate hard-sphere density $V_0/V=0.25$, as a function of kl_E from BGK with $M=35$. Heat mode (· · · ·), two sound modes (——), and two kinetic modes (— — —), which are propagating for $kl_E > 0.2$.

D. Large k

As for the dilute gas and the dense fluid, no simplified description of the correlation functions is possible for $1 < kl_E < 3$. However, for $3 < kl_E < \infty$, the ideal gas plus a single binary collision correction due to Λ^s [cf. Eq. (4.13)] again provides a good approximation to the $S_{\alpha\beta}(k,\omega)$, as is shown in Fig. 10.

VI. DISCUSSION

We end with a number of remarks.

(1) A phase diagram can be made in the density—wave-vector plane illustrating the different regions, where different dynamical processes dominate the behavior of the hydrodynamic correlation functions. This is done in Fig. 11. In this figure it is indicated that, beyond the hydrodynamic region, the correlation functions $S_{\alpha\beta}(k,\omega)$ of the fluid can be described up to $kl_E \approx 1$ by three or five (either true or effective) extended modes; that for $1 < kl_E < 3$ the $S_{\alpha\beta}(k,\omega)$ are most conveniently obtained using matrix inversion [cf. Eqs. (2.24) and (2.27)]; and that for $kl_E > 3$, the $S_{\alpha\beta}(k,\omega)$ are described by their ideal-gas values and a

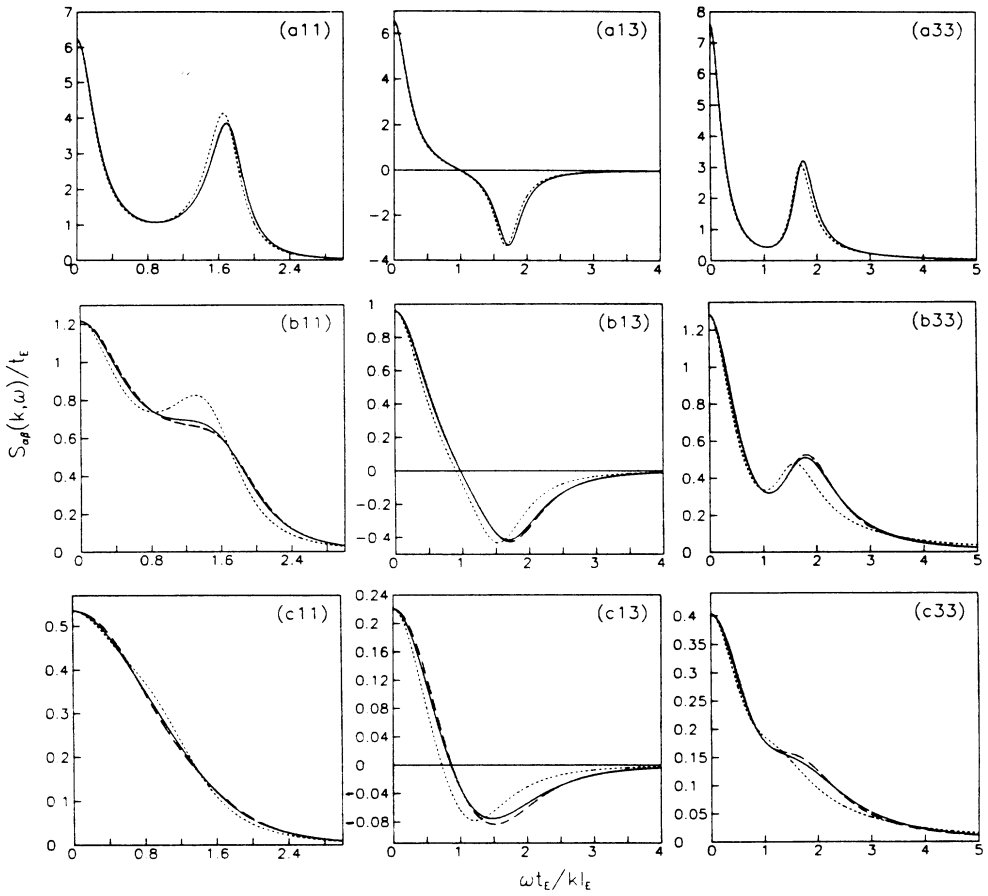

FIG. 9. Intermediate-density hard-sphere gas, $V_0/V=0.25$, correlation functions $S_{\alpha\beta}(k,\omega)/t_E$ (——) as a function of $\omega t_E/kl_E$, from BGK matrix inversion with $M=35$. Letters and numbers as in Fig. 2 with l_0,t_0 replaced by l_E,t_E. . . ., with three effective modes; — — —, with five effective modes. In (a11) and (b11), the contributions of the three extended hydrodynamic heat and sound modes from BGK with $M=35$ are indistinguishable from the $S_{11}(k,\omega)/t_E$ (——).

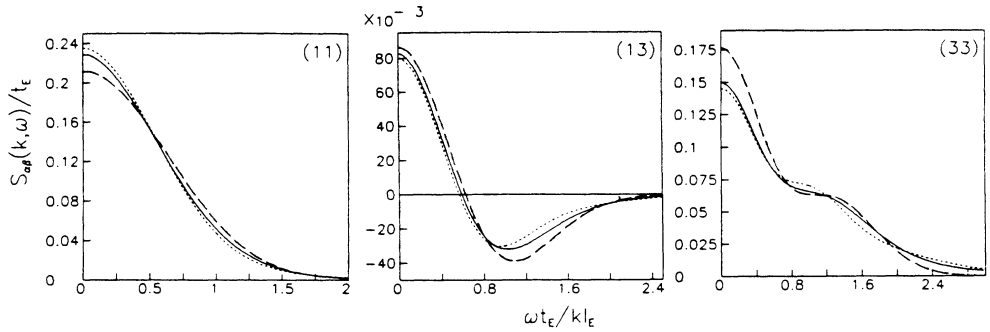

FIG. 10. Intermediate-density hard-sphere gas, $V_0/V=0.25$, correlation functions $S_{\alpha\beta}(k,\omega)$ as a function of $\omega t_E/kl_E$ for $kl_E=3$. For the curves see Fig. 7.

correction due to a single binary collision [cf. Eqs. (3.4) and (4.13)]. At low densities this correction is given by the Boltzmann collision operator for $kl_E>3$, while after a transition region, for $kl_E\gg 3$ it is determined by the Lorentz-Boltzmann operator (cf. Fig. 11). Thus, for example, at the low density of $V_0/V=0.015$, this transition region comprises $10<kl_E<50$, which corresponds to $1\leqq k\sigma\leqq 5$, since $l_E/\sigma=10$. It might be interesting to see if such a transition region at large k can be observed in neutron scattering experiments.

(2) The description of the correlation functions $S_{\alpha\beta}(k,\omega)$ for $0\leqq kl_E<1$ by the $\bar{S}^{e}_{\alpha\beta}(k,\omega)$ with five effective modes [cf. Eq. (5.3)], derived here for intermediate densities, can also be used at high and at low densities. At high densities the two extra (kinetic) modes do not affect the three effective mode result, but at low densities around $V_0/V\sim 0.1$, where the transition from dilute gas (Boltzmann) behavior to intermediate-density behavior takes place, they give better results than obtained with three true modes. For the dilute gas five effective modes give a representation comparable to that of three true modes, except for S_{33} at $kl_0=0.8$, where five modes are considerably better.

(3) The ω dependence of the $S_{\alpha\beta}(k,\omega)$ is studied in this paper only for the reduced frequency range $0\leqq\omega t_E/kl_E\approx O(1)$. This implies that the representations for the $S_{\alpha\beta}(k,\omega)$ considered here are not necessarily valid for $\omega\to\infty$. For example, while the exact $S(k,\omega)$ decays proportional to ω^{-4} for large ω,[22] the representation of $S(k,\omega)$ with three true modes decays proportional to ω^{-2} when $\omega\to\infty$.

Such differences are irrelevant, however, when one restricts oneself to a description of the $S_{\alpha\beta}(k,\omega)$, in the limited frequency range used here.

(4) Not only hydrodynamic correlation functions but all correlation functions between single particle functions of the general form $\sum_{i=1}^{N} f(\mathbf{v}_i)\delta(\mathbf{r}-\mathbf{r}_i)$ can be computed with the BGK method discussed here, since any $f(\mathbf{v}_i)$ can be expanded in terms of the complete orthonormal set $\{\phi_i\}$, so that all $F^{E}_{jl}(k,t)$ can be computed, using the BGK method.

(5) We have made a comparison of the 3×3 generalized effective hydrodynamic matrix $\underline{H}^{e}(k)$ [cf. Eq. (4.6)] calculated here from the revised Enskog theory with that, $\underline{H}^{e'}(k)$, obtained by Alley and Alder from their computer simulations.[18]

To do so, we express, following Alley and Alder, the effective hydrodynamic matrix of a hard-sphere fluid in terms of the hard-sphere static structure factor $S(k)$, the generalized ratio of specific heats $\gamma(k)$, the generalized longitudinal viscosity $\alpha(k)$, and the generalized thermal conductivity $\lambda(k)$, so that

$$\underline{H}^{e'}(k)=\begin{vmatrix} 0 & i\omega_0(k) & 0 \\ i\omega_0(k) & \alpha(k)k^2 & i\omega_0(k)[\gamma(k)-1]^{1/2} \\ 0 & i\omega_0(k)[\gamma(k)-1]^{1/2} & \dfrac{\lambda(k)k^2}{nc_v} \end{vmatrix}, \tag{6.1}$$

where $\omega_0(k)=k[k_BT/mS(k)]^{1/2}$ and $c_v=3k_B/2$. For $k\to 0$, $\gamma(0)=\gamma=c_p/c_v$, $\alpha(0)=\alpha=(\frac{4}{3}\eta+\zeta)$ the longitudinal viscosity, with η and ζ the shear and bulk viscosities of the fluid, respectively, and $\lambda(0)=\lambda$ the thermal conductivity. Then, using Alley and Alder's tabulated values for $S(k)$, $\gamma(k)$, $\alpha(k)$, an $\lambda(k)$ at $V_0/V=0.1$, 0.333, and 0.625, we determined the eigenvalues $z_h(k),z_{\pm}(k)$ of $\underline{H}^{e'}(k)$ for these three densities. The results so obtained for the heat mode $z_h(k)$, the sound dispersion $\omega_s(k)=|\mathrm{Im}z_{\pm}(k)|$, and the sound damping $z_s(k)=\mathrm{Re}z_{\pm}(k)$ are compared in Fig. 12, with those calculated with the revised Enskog theory.

We see in Figs. 12(a) and (12b) that the revised Enskog theory describes the z_h, ω_s, and z_s of a real hard-sphere fluid well, both for the low density $V_0/V=0.1$ and the intermediate density $V_0/V=0.333$.

We conclude therefore that an Enskog fluid closely resembles a real hard-sphere fluid for $V_0/V=0.1$ and 0.333. A comparison of the $z_h(k)$, $\omega_s(k)$, and $z_s(k)$ of the Enskog fluid and the real hard-sphere fluid at the high

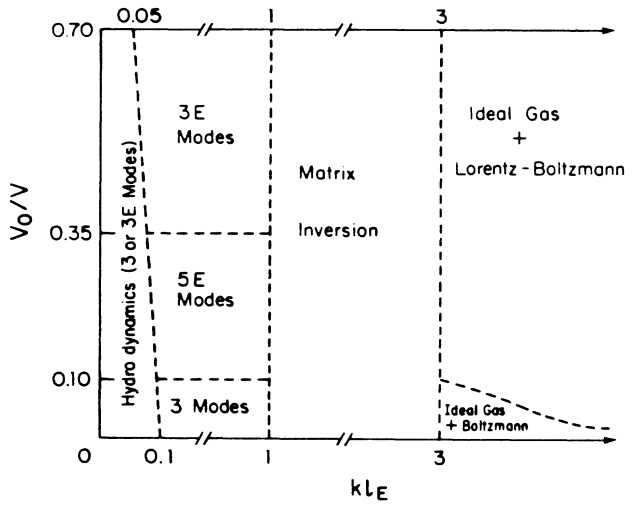

FIG. 11. Phase diagram in the space of the reduced density (V_0/V) and the reduced wave number (kl_E), as discussed in Sec. VI, subparagraph (1) in the text. Indicated are regions where particular approximations give good representations of the correlation functions. The dotted lines indicate transition regions.

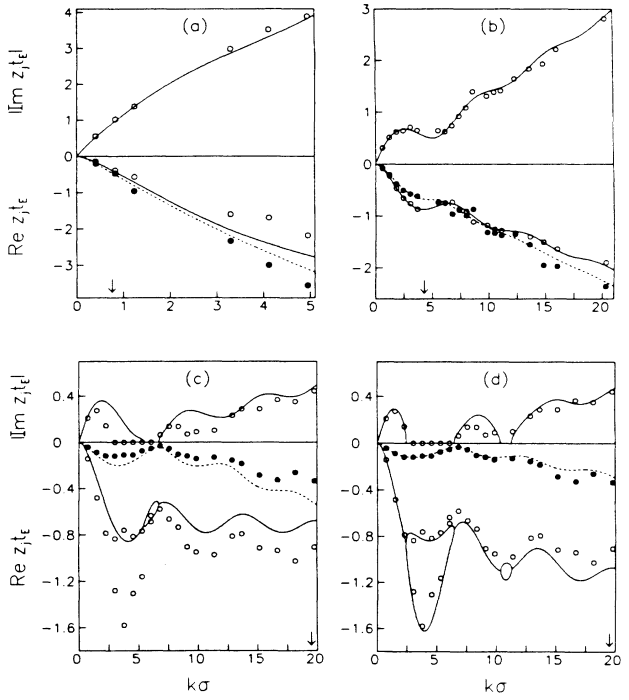

FIG. 12. Comparison of the Enskog theory with the hard-sphere molecular dynamics data of Alley and Alder. Plotted are the reduced eigenvalues of the generalized hydrodynamic matrix of Alley and Alder (●, heat mode; ○, sound modes) and the theoretical three effective hydrodynamic heat (· · · ·) and sound (——) modes. (a) $V_0/V=0.1$; (b) $V_0/V=0.333$; (c) $V_0/V=0.625$; (d) $V_0/V=0.625$, with upgraded longitudinal viscosity and thermal conductivity. The arrows indicate that value of $k\sigma$ for which $kl_E=1$.

density $V_0/V=0.625$ has been made before.[16] The agreement is less satisfactory than that at $V_0/V=0.1$ and 0.333, especially for the sound damping [cf. Fig. 12(c)]. This difference between the Enskog and a real hard-sphere fluid with increasing densities might be due mainly to a difference in their shear viscosities.

To see this, we remark that in the revised Enskog theory $\underline{H}^e(k)$ is given by an equation similar to Eq. (6.1), with $\gamma(k)$, $\alpha(k)$, and $\lambda(k)$ replaced by their corresponding Enskog values $\gamma_E(k)$, $\alpha_E(k)$, and $\lambda_E(k)$, respectively. Here $\gamma_E(0)=\gamma(0)=\gamma$, $\alpha_E(0)=\alpha_E=(\frac{4}{3}\eta_E+\zeta_E)/mn$ with α_E, η_E, and ζ_E the Enskog values of the longitudinal, shear, and bulk viscosities, respectively, and $\lambda_E(0)=\lambda_E$, the Enskog heat conductivity. While for $V_0/V=0.1$ and 0.333, α and λ are within a few percent of α_E and λ_E, respectively, for $V_0/V=0.625$, $\alpha/\alpha_E=1.55$, and $\lambda/\lambda_E=1.05$ so that in particular α and α_E differ considerably.[18] We believe that this is the origin of the disagreement between Enskog and real hard-sphere fluids at high densities also for $k>0$. For, multiplying in the $\underline{H}^e(k)$ of the revised Enskog theory, the Enskog values $\alpha_E(k)$ and $\lambda_E(k)$ with the constant factors 1.55 and 1.05 relevant for $k=0$, respectively, a considerably better agreement is obtained at $V_0/V=0.625$ up to $k\sigma=20$ between the thus "upgraded" $z_h^e(k)$, $\omega_s^e(k)$, and $z_s^e(k)$ and those derived from Alley and Alder's computer simulations [cf. Fig. 12(d)].

This agreement means that our computed *theoretical* correlation functions for the Enskog fluid using three effective modes are identical to the *experimental* correlation functions determined by Alley and Alder for real hard-sphere fluids for those densities and k values, where three effective modes suffice. Then the dynamical processes that determine the nine hydrodynamic correlation functions are characterized by three effective hydrodynamic modes.

It seems possible that the large ratio $\alpha(k)/\alpha_E(k)=1.55$ for $k=0$ as well as for larger values of k can be understood on the basis of the same extended mode coupling theory that has successfully explained the large ratio $\eta/\eta_E=1.44$ of the shear viscosities of the real hard-sphere and Enskog fluids at $V_0/V=0.625$.[35–37]

(6) In view of its special importance, we conclude with a few remarks on $S(k,\omega)$ alone.

First, we note that for hard spheres for all densities and $kl_E<1$, $S(k,\omega)$ alone can always be described by three modes, which are either true or effective modes, depending on density and k value (cf. Figs. 2, 6, and 9). The physical interpretation of these modes, as to what physical processes they represent, has been the main point of this paper.

Second, we note that also for real fluids, like argon[6] or neon,[7] as well as for Lennard-Jones fluids,[38] $S(k,\omega)$ can always be represented by three Lorentzians, i.e., by three modes. Since there is no kinetic theory of real fluids, like the revised Enskog theory for hard-sphere fluids, an inter-

pretation of these three modes in terms of physical processes as a function of density, and wave number k, in a similar fashion as was done here for hard-sphere fluids, is much more complicated.[39]

ACKNOWLEDGMENT

This work was supported by the U.S. Department of Energy under Contract No. DE-AC02-81ER10807.

*Permanent address: Center for Automation Reseach, University of Maryland, College Park, MD 20742.

†Permanent address: Interuniversitair Reactor Instituut, Mekelweg 15, NL-2629 JB Delft, Zuid-Holland, The Netherlands.

[1]N. A. Clark, Phys. Rev. A **12**, 232 (1975).

[2]J. P. Boon and S. Yip, *Molecular Hydrodynamics* (McGraw-Hill, New York, 1980).

[3]K. Sköld, J. M. Rowe, G. Ostrowski, and P. D. Randolph, Phys. Rev. A **6**, 1107 (1972).

[4]J. R. D. Copley and J. M. Rowe, Phys. Rev. A **9**, 1656 (1974).

[5]P. A. Egelstaff, W. Gläser, D. Litchinski, E. Schneider, and J.-B. Suck, Phys. Rev. A **27**, 1106 (1983).

[6]A. A. van Well, P. Verkerk, L. A. de Graaf, J.-B. Suck, and J. R. D. Copley, Phys. Rev. A **31**, 3391 (1985).

[7]A. A. van Well and L. A. de Graaf, Phys. Rev. A **32**, 2396 (1985).

[8]J. L. Lebowitz, J. K. Percus, and J. Sykes, Phys. Rev. **188**, 487 (1969).

[9]H. H. U. Konijnendijk and J. M. J. van Leeuwen, Physica **64**, 342 (1973).

[10]H. van Beijeren and M. H. Ernst, Physica **68**, 437 (1973); J. Stat. Phys. **21**, 125 (1979).

[11]G. F. Mazenko, Phys. Rev. A **7**, 209 (1973); **7**, 222 (1973); **9**, 360 (1974).

[12]P. M. Furtado, G. F. Mazenko, and S. Yip, Phys. Rev. A **12**, 1653 (1975); **13**, 1641 (1976).

[13]I. M. de Schepper and E. G. D. Cohen, Phys. Rev. A **22**, 287 (1980).

[14]I. M. de Schepper and E. G. D. Cohen, J. Stat. Phys. **27**, 223 (1982).

[15]E. G. D. Cohen, I. M. de Schepper, and M. J. Zuilhof, Physica B **127**, 282 (1984); Phys. Lett. **101A**, 399 (1984); **103A**, 120 (1984).

[16]E. G. D. Cohen, B. Kamgar-Parsi, and I. M. de Schepper, Phys. Lett. **114A**, 241 (1986).

[17]B. Kamgar-Parsi and E. G. D. Cohen, Physica A **138**, 249 (1986).

[18]W. E. Alley and B. J. Alder, Phys. Rev. A **27**, 3158 (1983).

[19]W. E. Alley, B. J. Alder, and S. Yip, Phys. Rev. A **27**, 3174 (1983).

[20]C. Bruin, J. P. J. Michels, J. C. van Rijs, L. A. de Graaf, and I. M. de Schepper, Phys. Lett. **110A**, 40 (1985).

[21]M. H. Ernst, J. R. Dorfman, W. R. Hoegy, and J. M. J. van Leeuwen, Physica **45**, 127 (1969).

[22]I. M. de Schepper, M. H. Ernst, and E. G. D. Cohen, J. Stat. Phys. **25**, 321 (1981).

[23]E. G. D. Cohen and I. M. de Schepper, J. Stat. Phys. (to be published).

[24]J. D. Foch and G. W. Ford, in *Studies in Statistical Mechanics,* edited by J. de Boer and G. E. Uhlenbeck (North-Holland, Amsterdam, 1970), Vol. V, part B, p. 101.

[25]Z. Alterman, K. Frankowski, and C. S. Pekeris, Astrophys. J., Suppl. Ser. **69**, 291 (1962).

[26]B. D. Fried and S. D. Conte, *The Plasma Dispersion Function* (Academic, New York, 1961).

[27]S. Chapman and T. G. Cowling, *The Mathematical Theory of Nonuniform Gases* (Cambridge University Press, Cambridge, 1970).

[28]J. J. Erpenbeck (private communication).

[29]M. A. Burschka and E. G. D. Cohen (unpublished).

[30]E. G. D. Cohen, in *Trends in Applications of Pure Mathematics to Mechanics,* Vol. 249 of *Lecture Notes in Physics,* edited by E. Kröner and K. Kirchgässer (Springer-Verlag, Berlin, 1986), pp. 3–24.

[31]T. R. Kirkpatrick, Phys. Rev. A **32**, 3130 (1985).

[32]W. Montfrooy, P. Verkerk, and I. M. de Schepper, Phys. Rev. A **33**, 540 (1986).

[33]J. R. D. Copley and S. W. Lovesey, Rep. Progr. Phys. **38**, 461 (1975).

[34]S. W. Lovesey, Phys. Rev. Lett. **53**, 401 (1984); Z. Phys. B **58**, 79 (1985).

[35]T. R. Kirkpatrick, Phys. Rev. Lett. **53**, 1735 (1984); 2185 (1984).

[36]T. R. Kirkpatrick and J. C. Nieuwoudt, Phys. Rev. A **33**, 2651 (1986).

[37]I. M. de Schepper, A. F. E. M. Haffmans, and H. van Beijeren, Phys. Rev. Lett. **56**, 538 (1986); **57**, 1715 (1986).

[38]I. M. de Schepper, J. C. van Rijs, A. A. van Well, P. Verkerk, L. A. de Graaf, and C. Bruin, Phys. Rev. A **29**, 1602 (1984).

[39]I. M. de Schepper, J. C. van Rijs, W. Montfrooy, L. A. de Graaf, C. Bruin, and E. G. D. Cohen (unpublished).